JOURNAL OF SOLID STATE CHEMISTRY 44, 192–200 (1982)

The Effects of Titanium or Chromium Doping on the Crystal Structure of V_2O_3

SAMUEL CHEN, JAMES E. HAHN, CATHERINE E. RICE, AND WILLIAM R. ROBINSON*

Department of Chemistry, Purdue University, West Lafayette, Indiana 47907

Received February 19, 1982

The crystal structures of five samples of $(Ti_xV_{1-x})_2O_3$ ($0.011 \leq x \leq 0.077$) and seven samples of $(Cr_xV_{1-x})_2O_3$ (both metallic and insulating phases, $0 \leq x \leq 0.05$) were determined from X-ray diffraction data collected from single crystals. These compounds are isomorphous with α-alumina. The cell dimensions change such that the a axes increase and the c axes decrease with increasing Ti or Cr. In the $Cr-V_2O_3$ system, from 0 to 1.25% Cr doping, changes in structure parallel those observed in the $Ti-V_2O_3$ system. These changes are consistent with a slight weakening of the bonding metal–metal interactions in the basal plane, leading to an increase in the metal–metal distances coupled with changes which maintain constant metal–oxygen distances. A discontinuity appears at about 1.25% Cr as the transition from metal to insulating behavior occurs with increasing Cr content. No change in crystal symmetry accompanies this transformation. It appears that the metal–metal bonding interactions are retained even in the insulating phase of Cr-doped V_2O_3. A comparison of the structural variation in the Cr- and Ti-doped systems suggests that the change from metallic to insulating behavior cannot be a structure effect. These changes are, however, consistent with the band model proposed by others for these systems.

Introduction

Pure vanadium sesquioxide, V_2O_3, exhibits at least three different types of electrical behavior with attendant structural features. At low temperatures it forms a monoclinic, antiferromagnetic insulating (AFI) phase (*1*). Upon warming to about 160K, a first-order phase transition to a metallic phase with the corundum structure (α-Al_2O_3) is observed (*2*). At higher temperature (about 300–600K) a continuous increase in resistivity of about 1 order of magnitude is seen (*3*). The transition from the metallic (M) to the high-temperature (HT) corundum phase is accompanied by a continuous change in the dimensions of the crystal structure but by no change in crystal symmetry (*4, 5*).

The addition of increasing amounts of Ti_2O_3 to V_2O_3 continuously suppresses both the low-temperature and high-temperature transitions (*6*). Above 5.5% Ti_2O_3 the solid solution is metallic at all temperatures examined. Those V_2O_3 phases (M and HT) with the corundum structure retain this structure upon addition of Ti_2O_3, although small changes in cell dimensions have been reported (*7, 8*).

Addition of up to about 0.5% of Cr_2O_3 or Al_2O_3 to pure V_2O_3 produces solid solutions which closely mimic the behavior of pure V_2O_3, although the transition temperatures shift slightly and the resistivity increases by about 10 to 15% (*9, 10*). With about 0.5 to

* Author to whom correspondence should be addressed.

0022-4596/82/110192-09$02.00/0

2% Cr_2O_3 or Al_2O_3, a first-order transition between the M and HT phases is observed. This first-order transition occurs at progressively lower temperatures and the resistivity of the accompanying M phase increases by over an order of magnitude with increasing dopant concentrations. Above a dopant level of about 2%, the M phase is no longer observed and the AFI phase transforms directly to the HT phase. Both the M and HT phases of Cr- or Al-doped V_2O_3 crystallize in the corundum structure with the dimensions of the M phases close to those of V_2O_3 at room temperature and the dimensions of the HT phases similar to those of pure V_2O_3 at elevated temperatures (*4, 5, 11*).

In view of the very different physical behavior of the Ti–V_2O_3 and Cr–V_2O_3 systems, we undertook a single-crystal X-ray diffraction study of a series of Ti-doped and Cr-doped V_2O_3 samples (both M and HT phases) at room temperature in order to determine if the structures of these materials reflect the differences in their electrical behavior.

Experimental

Samples of Cr–V_2O_3 [$(Cr_xV_{1-x})_2O_3$ with x = 0.0000, 0.0015, 0.0030, 0.0037, 0.0045, 0.0052, 0.0060, 0.0100, 0.0125, 0.0200, 0.0300, and 0.0500] were grown by the Tri-Arc Czochralski method at the Purdue University Crystal Growth Center. V_2O_3 was prepared by reducing 99.995% pure V_2O_5 (from Puratronic) in a stream of H_2 for several days at 873K. The requisite amounts of V_2O_3 and 99.999% pure Cr_2O_3 (from Atomergic) were melted together under gettered argon. Single-crystal boules were pulled from the melt using a seed of the same composition as the melt. Upon cooling, the M phase was recovered for V_2O_3 to 0.60% Cr–V_2O_3. The other samples remained in the HT phase. M-phase 1.00 and 1.25% Cr–V_2O_3 was obtained by cooling samples at 230K for 12 hr.

Samples of Ti–V_2O_3 [$(Ti_xV_{1-x})_2O_3$ with x = 0.011, 0.030, 0.045, 0.055, and 0.077] were made in a similar fashion using Ti_2O_3 as the dopant. Ti_2O_3 was prepared by arc-melting together appropriate quantities of 99.99% pure Ti (Atomergic) and 99.998% pure TiO_2 (Puratronic). Details of this crystal growth technique are described elsewhere (*12*). It has been shown (*13*) that the resulting V/Cr and V/Ti ratios in these boules are within 1% of the actual ratio as weighed out prior to melting.

Spherical crystals with radii of about 0.01 cm were ground from fragments of the boules and mounted along nonprincipal axes to reduce the effects of multiple diffraction. Unit cell parameters and intensities were measured using an Enraf-Nonius CAD-4 automated diffractometer with graphite monochromated Mo$K\alpha$ radiation.

Precise unit cell dimensions of M-phase $(Cr_xV_{1-x})_2O_3$, $0 \leq x \leq 0.0125$, and of the HT phase, $0.0100 \leq x \leq 0.0500$, as well as those of $(Ti_xV_{1-x})_2O_3$, $0.011 \leq x \leq 0.077$, were determined by centering with $K\alpha_1$ (λ = 0.70926 Å) peak for 50 to 60 reflections with $80° < |2\Theta| < 100°$ at both positive and negative 2Θ and taking the average as the diffraction angle. Hexagonal cell parameters and their esd's (Table I) were calculated by least-squares refinement of the observed 2Θ values (*14*). Numbers given in these tables are averaged cell dimension values. Measurement on two to four spherical crystals per boule were used to examine its homogeneity and all values from the same boule matched within 2 esd's, except for x = 0.0030 of $(Cr_xV_{1-x})_2O_3$ in which the agreement was to 3 esd's.

For x = 0.0052, 0.0100, 0.0125 in the M phase and for x = 0.0100, 0.0125, 0.030, and 0.0500 in the HT phase of $(Cr_xV_{1-x})_2O_3$ and for all samples of the $(Ti_xV_{1-x})_2O_3$ system, an X-ray intensity data set was collected for h, $\pm k$, $\pm l$ reflections of the hexagonally indexed rhombohedral unit cell. Except for the M and HT form of 1.00% Cr–V_2O_3 each intensity data set was gathered and treated in the following manner.

All reflections in the hemisphere of reciprocal space with $6° < 2\Theta < 66°$ were col-

TABLE I

HEXAGONAL UNIT CELL DIMENSIONS OF DOPED V_2O_3 WITH STANDARD DEVIATIONS

	Atomic % dopant	a (Å)	c (Å)	c/a	Volume (Å^3)
Ti–V_2O_3					
	0	4.9532(2)	14.006(2)	2.828	297.59
	1.1	4.9572(1)	14.005(1)	2.825	298.05
	3.0	4.9633(1)	14.000(1)	2.820	298.67
	4.5	4.9671(1)	13.996(1)	2.818	299.03
	5.5	4.9714(2)	13.996(1)	2.815	299.56
	7.7	4.9752(2)	13.996(1)	2.813	300.02
	10.0[a]	4.9813(2)	13.996(1)	2.810	300.76
LT Cr–V_2O_3					
	0.15	4.9534(2)	14.003(1)	2.827	297.55
	0.30	4.9536(2)	14.005(2)	2.827	297.62
	0.37	4.9536(2)	14.004(1)	2.827	297.59
	0.45	4.9536(2)	14.005(2)	2.827	297.62
	0.52	4.9540(3)	14.003(2)	2.827	297.62
	0.60	4.9543(2)	14.002(2)	2.826	297.64
	1.00	4.9558(2)	13.998(1)	2.824	297.73
	1.25	4.9561(2)	13.998(1)	2.824	297.77
HT Cr–V_2O_3					
	1.00	4.9961(2)	13.936(2)	2.789	301.25
	1.25	4.9978(3)	13.932(2)	2.788	301.37
	2.00	4.9988(2)	13.927(1)	2.786	301.38
	3.00	4.9989(2)	13.924(1)	2.785	301.33
	5.00	4.9989(2)	13.919(2)	2.784	301.22

[a] From Ref. (*8*).

lected in the $\Omega - 2\Theta$ scanning mode. Details of this type of data collection are described elsewhere (*8*). Three standard reflections were monitored at intervals of 60 reflections, and they did not show significant intensity changes during the course of each data collection period. Approximately 640 reflections were measured for each data set, which was then corrected for background, Lorentz polarization, and spherical absorption effects using μR values which ranged from 0.95 to 1.44. Subsequent averaging of equivalent reflections gave about 125 symmetry-independent reflections for each sample.

For the M and HT forms of 1.00% Cr–V_2O_3, a data set which was collected for valence electron density measurement was used. Data was collected in a hemisphere of reciprocal space with $6° < 2\Theta < 150°$. Adjustments for background, Lorentz polarization, and spherical absorption effects were made, but the equivalent reflections were not averaged. As a result, 2384 reflections for the M phase and 2554 reflections for the HT phase were used for the subsequent structural refinements.

Full matrix least-squares refinement with anisotropic temperature factors was carried out for each set of intensity data using the RFINE-2 program written by Finger (*15*). The initial atomic parameters in the space group $R\bar{3}c$ were those for $(Cr_{0.01}V_{0.99})_2O_3$ (*5*). The program minimized $\Sigma w (F_o - F_c)^2$ using the scattering factors for V^{3+}, Cr^{3+}, and O^0 (*16*) corrected for real and imaginary anomalous dispersion, weights based on the error determined in the averaging process [$w = 1/\sigma^2(F) = 4F_o^2/\sigma^2(F^2)$] or on counting statistics for 1% Cr–V_2O_3, and an

isotropic extinction correction of the form $F_{corr} = F_0 (1 + sI_0)$. Final R values ranged from 0.014 to 0.038. Values of the standard deviation of an observation of unit weight are listed in Tables II and III as S. The final atom parameters listed in these tables were used with their variance–covariance matrices to calculate the interatomic distances and bond angles and their esd's.

Results

All of the Cr- and Ti-doped systems studied were found to be isostructural with corundum (α-Al_2O_3). The structures consist of a distorted hexagonally closest-packed array of oxide ions with metal ions occupying two-thirds of the octahedral sites (Fig. 1). If the structure were in the ideal HCP arrangement, both z for the metal ion and x for the oxygen ion would be one-third. Each metal ion [for example, M(1) in Fig. 1] has four near metal neighbors; one sharing an octahedral face of the coordination polyhedron [M(2) in Fig. 1] and three sharing edges of the octahedron [M(3) in Fig. 1 and two symmetry-related ions].

Unit Cell Dimensions

The values of the unit cell parameters in these systems at various compositions are presented in Table I. Since these cell parameters were all determined on the same instrument under the same conditions, differences in systematic errors between samples were minimized (*8*).

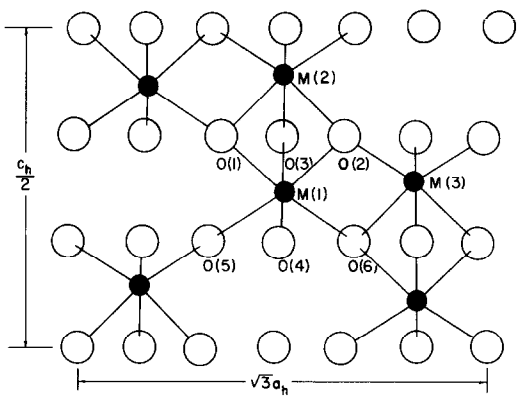

FIG. 1. A projection of the corundum structure on a plane perpendicular to the [110] axis.

Addition of increasing amounts of Ti_2O_3 to V_2O_3 results in a smooth increase in a in the hexagonally indexed rhombohedral cell (Table I). The c axis decreases initially, but at about 4.5% Ti it assumes a constant value which does not change until the Ti concentration exceeds 50% (*8*). The change in a is +0.6% in the 0 to 10% Ti range. That of the c axis is −0.1% in the 0 to 4.5% Ti range, after which c does not change.

Between a Cr concentration of 0 and 1.25%, the a dimension of M Cr–V_2O_3 increases from 4.9532(1) to 4.9561(2) Å, while c decreases from 14.006(2) to 13.998(1) Å. The corresponding values interpolated for 1.25% Ti–V_2O_3 are 4.9577 and 14.005 Å, respectively.

An increase of about 0.8% in a and a decrease of about 0.5% in c accompany the change from the M to the HT phase in 1.00% Cr–V_2O_3 and 1.25% Cr–V_2O_3. The cell volume increases by about 1.2% during this transition. Both phases can be obtained at room temperature because of the large hysteresis in the transition temperature. With increasing Cr content, the c dimension of HT Cr–V_2O_3 decreases by about 0.1% over the range from 1.25 to 5% Cr. The a dimension changes very little above 2% Cr. It is interesting to note that the slopes of the cell dimensions vs percentage Cr appear to differ in the region from 1 to 2% Cr and 2 to 5% Cr. In the 1 to 2% Cr range, Cr–V_2O_3 exhibits a first-order M–HT transition, while in the higher concentration range it does not.

Increasing both the Ti and Cr content reduces the value of c/a in these solid solutions as does the M–HT transition. All of these samples have anomalously high c/a ratios, however (*vide infra*).

Interatomic Distances

Addition of up to 10% Ti_2O_3 to V_2O_3 results in a smooth increase in the M(1)–M(2) distance across the shared octahedral face and in the M(1)–M(3) distance across

TABLE II

CRYSTALLOGRAPHIC DATA FOR $(Ti_xV_{1-x})_2O_3$, DISTANCES, AND ANGLES WITH STANDARD DEVIATIONS IN PARENTHESES

	V_2O_3[a]	1.1% Ti	3% Ti	4.5% Ti	5.5% Ti	7.7% Ti	10% Ti[b]
M : z	0.34634(4)	0.34644(3)	0.34665(5)	0.34677(4)	0.34680(2)	0.34686(2)	0.34691(4)
β_{11}	57(6)[c]	41(2)	49(5)	35(4)	55(2)	52(2)	56(3)
β_{33}	1.9(7)	3.4(3)	1.2(5)	2.0(6)	4.5(2)	4.8(2)	4.4(4)
Ox : x	0.3122(5)	0.3114(3)	0.3115(5)	0.3112(4)	0.3106(3)	0.3106(3)	0.3110(4)
β_{11}	49(10)	48(5)	56(9)	41(7)	57(4)	54(5)	55(7)
β_{22}	76(14)	58(7)	63(12)	52(10)	67(6)	64(7)	58(10)
β_{33}	5.0(10)	5.2(5)	4.1(10)	5.0(9)	6.2(5)	6.5(5)	5.7(7)
β_{13}	4(2)	2.8(9)	3.4(13)	3.1(11)	1.9(8)	2.3(9)	4.1(11)
R_{wt}	0.039	0.018	0.028	0.025	0.015	0.014	0.017
R	0.048	0.021	0.039	0.033	0.017	0.018	0.025
n	98	133	133	133	133	133	120
$S(\times 10^5)$		3.9(2)	6.1(5)	7.6(6)	1.6(1)		1.8(2)
			Distances				
M(1)–M(2)	2.697(1)	2.701(1)	2.706(1)	2.708(1)	2.710(1)	2.711(1)	2.713(1)
M(1)–M(3)	2.880(1)	2.885(1)	2.890(1)	2.892(1)	2.895(1)	2.897(1)	2.901(1)
M(1)–O(1)	2.051(1)	2.051(1)	2.054(1)	2.055(1)	2.054(1)	2.056(1)	2.059(1)
M(1)–O(5)	1.968(1)	1.972(1)	1.972(1)	1.973(1)	1.975(1)	1.976(1)	1.977(1)
O(1)–O(2)	2.676(3)	2.674(3)	2.678(3)	2.677(2)	2.674(2)	2.676(2)	2.683(2)
O(1)–O(4)	2.804(1)	2.805(1)	2.805(1)	2.805(1)	2.804(1)	2.805(1)	2.807(1)
O(1)–O(5)	2.889(1)	2.893(1)	2.893(1)	2.894(1)	2.896(1)	2.897(1)	2.898(1)
O(4)–O(5)	2.952(1)	2.960(1)	2.964(2)	2.968(1)	2.973(1)	2.975(1)	2.977(2)
			Angles				
O(1)–M(1)–O(2)	81.45(7)	81.35(7)	81.34(6)	81.29(7)	81.23(6)	81.23(6)	81.32(6)
O(1)–M(1)–O(4)	88.46(2)	88.38(2)	88.30(2)	88.24(2)	88.18(2)	88.14(2)	88.10(2)
O(1)–M(1)–O(5)	91.90(5)	91.94(4)	91.86(5)	91.84(4)	91.87(4)	91.84(4)	91.75(4)
O(1)–M(1)–O(6)	168.62(8)	168.45(7)	168.33(7)	168.22(8)	168.11(7)	168.07(7)	168.10(7)
O(4)–M(1)–O(5)	97.17(3)	97.29(3)	97.43(3)	97.54(3)	97.61(2)	97.66(3)	97.71(3)
M(1)–O(1)–M(2)	82.23(9)	82.36(9)	82.38(9)	82.44(8)	82.53(7)	82.52(7)	82.41(7)
M(1)–O(2)–M(3)	91.54(3)	91.62(2)	91.70(3)	91.76(2)	91.82(2)	91.85(2)	91.89(2)
M(2)–O(2)–M(3)	133.21(5)	133.25(4)	133.19(5)	133.18(5)	133.21(4)	133.20(4)	133.14(4)

[a] From Ref. (5).

[b] From Ref. (8).

[c] All β's $\times 10^4$. For M, $\beta_{11} = \beta_{22}$, $\beta_{12} = \frac{1}{2}\beta_{11}$, $\beta_{23} = \beta_{13} = 0$. For O, $\beta_{12} = \frac{1}{2}\beta_{22}$, $\beta_{23} = 2\beta_{13}$. The form of the anisotropic temperature factor T is $T = \exp(-\Sigma_i\Sigma_j h_i h_j \beta_{ij})$.

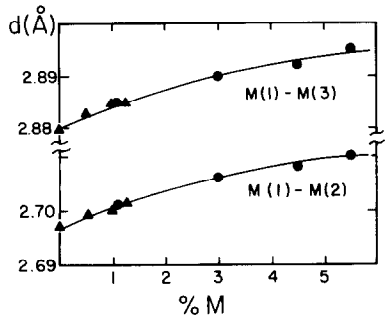

FIG. 2. Variation of metal–metal distance with percentage dopant: solid circles, Ti–V_2O_3; solid triangles, Cr–V_2O_3.

the shared octahedral edge (Table II and Fig. 2). At 10% Ti–V_2O_3, these distances have changed by 0.6 to 0.7%, 0.016 and 0.021 Å, respectively. The M–O distances have increased by 0.40 to 0.45% over the same range. With the exception of the increase in the O(4)–O(5) distances, the separations in the face opposite the shared face, the oxygen–oxygen distances change very little.

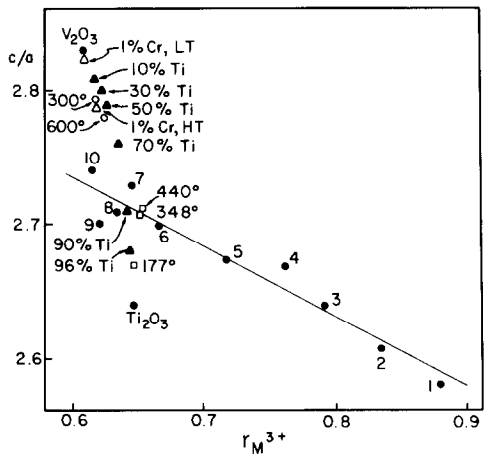

FIG. 3. Variation of c/a with ionic radius of the metal in corundum structures. Solid triangles, Ti–V_2O_3 [Ref. (*8*)]; open triangles, 1% Cr–V_2O_3 (M and HT forms); open squares, Ti_2O_3 upon heating [Ref. (*22*)]; open circles, V_2O_3 upon heating [Ref. (*5*)]; 1, Tl_2O_3; 2, $TlInO_3$; 3, In_2O_3; 4, $InScO_3$; 5, $InFeO_3$; 8, $GaFeO_3$; 9, Ga_2O_3 [Ref. (*19*)]; 6, Rh_2O_3 [A. Wold, R. J. Arnott, and W. J. Croft, *Inorg. Chem.* **2**, 972 (1963)]; 7, Fe_2O_3; 10, Cr_2O_3 [R. E. Newnham and Y. M. de Haan, *Z. Kristallogr.* **117**, 235 (1962)]; Ti_2O_3 [Ref. (*8*)]. Radii for 1–10 from R. D. Shannon and C. T. Prewitt, *Acta Crystallogr. Sect. B* **25**, 925 (1969).

Inasmuch as the composition of the M phase of Cr–V_2O_3 at room temperature is limited to a maximum Cr concentration of 1.25%, the net changes observed with varying Cr content in this phase are small and only just significant. However, it appears that the metal–metal distances are increasing (Table III and Fig. 2), M(1)–O(1) is not changing, and M(1)–O(2) is increasing with increasing Cr concentration. The metal–metal and metal–oxygen distances at the various Cr concentrations in M Cr–V_2O_3 are within 0.001 Å of those interpolated for the corresponding Ti concentrations in Ti–V_2O_3.

The first-order changes from M to HT Cr–V_2O_3 in the 1.00 and 1.25% doped samples are similar to those reported previously (*5*) for 1% Cr–V_2O_3. The M(1)–M(2) distances increase by 1.7%, about 0.045 Å (in spite of the decrease in the c axis of the cell); the M(1)–M(3) distances by 1.1%, about 0.03 Å; and the M(1)–O(1) and M(1)–O(5) distances by 0.5 and 0.3%, about 0.01 Å, respectively. The largest change in an oxygen–oxygen distance is that between O(4) and O(5), about 0.05 Å or 1.5%; O(1)–O(5) increases by about 0.01 Å and O(1)–O(2) and O(1)–O(4) decrease by about the same amount.

Changes in the structure of HT Cr–V_2O_3 with increasing Cr content are small. Between 1.00 and 5.00% Cr there appears to be a slight expansion of most distances except for O(1)–O(4) which appears to decrease. In general, the effect of adding more Cr to HT Cr–V_2O_3 is similar to that which results when Cr is added to M Cr–V_2O_3, in spite of the larger composition limits of the HT phase.

Discussion

The structural behavior in both the Ti–V_2O_3 and the Cr–V_2O_3 systems is striking in its deviation from Vegard's law. Doping with Cr^{3+}, a smaller ion than V^{3+}, results in an increase in the a dimension of the unit cell while doping with the larger Ti^{3+} ion

TABLE III

CRYSTALLOGRAPHIC DATA FOR $(Cr_xV_{1-x})_2O_3$, DISTANCES, AND ANGLES WITH STANDARD DEVIATIONS IN PARENTHESES

	M phase				HT phase			
	V_2O_3[a]	0.52% Cr	1.00% Cr	1.25% Cr	1.00% Cr	1.25% Cr	3.00% Cr	5.00% Cr
M : z	0.34634(4)	0.34637(5)	0.34647(1)	0.34648(2)	0.348481(4)	0.34856(3)	0.34867(4)	0.34866(4)
β_{11}	57(6)[b]	55(4)	65.0(3)	58(2)	60.6(1)	53(2)	50(2)	51(2)
β_{33}	1.9(7)	4.3(4)	5.12(3)	5.2(2)	5.35(1)	4.5(2)	4.6(3)	3.8(2)
Ox : x	0.3122(5)	0.3115(6)	0.3115(1)	0.3113(3)	0.30762(5)	0.3077(3)	0.3074(4)	0.3073(4)
β_{11}	49(10)	60(10)	75(1)	67(5)	70.1(5)	59(6)	60(6)	57(8)
β_{22}	76(14)	76(13)	79(2)	81(6)	72.8(7)	64(7)	62(8)	64(9)
β_{33}	5.0(10)	7.5(10)	6.8(2)	6.9(5)	7.31(6)	7.3(7)	7.6(7)	6.9(9)
β_{13}	4(2)	2.0(20)	2.2(2)	2.0(1)	1.68(8)	2.5(1)	2.7(1)	2.6(12)
R_{wt}	0.039	0.032	0.029	0.014	0.018	0.018	0.021	0.021
R	0.048	0.033	0.038	0.021	0.018	0.022	0.024	0.028
n	98	127	2384	127	2554	127	127	126
$S(\times 10^5)$		5.3(4)	3.99(2)	0.73(8)	1.92(2)	4.1(2)	5.6(3)	3.9(2)
				Distances				
M(1)–M(2)	2.697(1)	2.699(1)	2.7009(3)	2.701(1)	2.7449(1)	2.746(1)	2.748(1)	2.746(1)
M(1)–M(3)	2.880(1)	2.883(1)	2.8848(1)	2.885(1)	2.9152(2)	2.916(1)	2.917(1)	2.917(1)
M(1)–O(1)	2.051(1)	2.050(2)	2.0511(5)	2.050(1)	2.0605(2)	2.062(1)	2.061(1)	2.060(2)
M(1)–O(5)	1.968(1)	1.971(1)	1.9709(3)	1.972(1)	1.9766(1)	1.976(1)	1.976(1)	1.976(1)
O(1)–O(2)	2.676(3)	2.672(5)	2.6741(11)	2.673(2)	2.6620(4)	2.664(2)	2.662(3)	2.661(4)
O(1)–O(4)	2.804(1)	2.804(1)	2.8038(3)	2.803(1)	2.7940(1)	2.794(1)	2.792(1)	2.791(1)
O(1)–O(5)	2.889(1)	2.892(1)	2.8917(2)	2.892(1)	2.8980(1)	2.898(1)	2.897(1)	2.897(1)
O(4)–O(5)	2.952(1)	2.958(1)	2.9592(6)	2.961(1)	3.0019(3)	3.002(2)	3.004(2)	3.005(2)
				Angles				
O(1)–M(1)–O(2)	81.45(7)	81.37(8)	81.36(2)	81.34(4)	80.48(1)	80.48(5)	80.42(5)	80.43(6)
O(1)–M(1)–O(4)	88.46(2)	88.40(2)	88.37(1)	88.35(1)	87.56(1)	87.54(1)	87.49(2)	87.47(2)
O(1)–M(1)–O(5)	91.90(5)	91.95(6)	91.92(1)	91.92(3)	91.73(1)	91.69(4)	91.69(4)	91.69(5)
O(1)–M(1)–O(6)	168.62(8)	168.50(9)	168.44(2)	168.41(5)	166.63(1)	166.59(5)	166.49(6)	166.48(7)
O(4)–M(1)–O(5)	97.17(3)	97.24(4)	97.31(1)	97.33(2)	98.82(1)	98.87(2)	98.96(2)	98.97(3)
M(1)–O(1)–M(2)	82.23(9)	82.34(11)	82.35(3)	82.38(5)	83.53(1)	83.53(6)	83.60(7)	83.58(8)
M(1)–O(2)–M(3)	91.54(3)	91.60(2)	91.63(1)	91.65(1)	92.44(1)	92.46(1)	92.51(2)	92.53(2)
M(2)–O(3)–M(3)	133.21(5)	133.26(5)	133.23(1)	133.24(3)	133.07(1)	133.04(3)	133.04(3)	133.04(4)

[a] From Ref. (5).

[b] All β's $\times 10^4$. For M, $\beta_{11} = \beta_{22}$, $\beta_{12} = \frac{1}{2}\beta_{11}$, $\beta_{23} = \beta_{13} = 0$. For O, $\beta_{12} = \frac{1}{2}\beta_{22}$, $\beta_{23} = 2\beta_{13}$. The form of the anisotropic temperature factor T is $T = \exp(-\Sigma_i\Sigma_j h_i h_j \beta_{ij})$.

results, at least initially, in a decrease in the c dimension. However, a plot of unit cell volume versus effective ionic volume (where the ionic radius was determined by subtracting 1.400 Å from the average of the two metal–oxygen distances) is linear suggesting that there are no unusual packing effects in these structures. The behavior of the a and c axes can be attributed to anisotropic metal–metal bonding interactions in these compounds.

The atomic movements resulting from the addition of up to 1.25% Cr_2O_3 or up to 5.5% Ti_2O_3 to V_2O_3 appear to be in the same direction in spite of the fact that Ti^{3+} is larger and Cr^{3+} is smaller than V^{3+}. This structural behavior is consistent with a weakening of the basal plane metal–metal interaction upon doping with either Cr or Ti. The changes can be satisfactorily described as the result of the increase in the M(1)–M(3) distances coupled with reorganization of the structure in order to minimize changes in metal–oxygen distances. As the metal atoms in the basal plane [M(1)–M(3), Fig. 1] shift apart, the change in metal-bridging oxygen distances is minimized by an increase in the oxygen–oxygen separations in the unshared face of the coordination polyhedron [O(4), O(5), O(6)]. The O(1)–O(4) and O(1)–O(5) distances remain constant, so the unshared face and bridging face [O(1), O(2), O(3)] move closer together. Thus the lengthening of the a axis with increasing dopant content may be attributed to an increase in the M(1)–M(3) distance, while the contraction of the c axis reflects the shortening of the distances between the oxygen layers. With the oxygen atoms in the unshared face moving apart, the M(1)–M(2) distance must increase to maintain a constant M(1)–O(5) distance.

The electronic d state manifold of the metal ions in octahedral sites in a corundum structure is split in the C_3 crystalline field into an unstable σ antibonding pair of e^* orbitals, a pair of e_π orbitals directed toward three neighboring cations in the basal plane through common octahedral site edges, and an a_1 orbital directed along the c axis toward the one near neighboring cation through a common octahedral site face. The a_1 and e_π orbitals are metal–metal interacting orbitals and are believed to be energetically near the Fermi level (*17*).

Changes in bonding which would lead to the observed changes in metal–metal distances can be explained by the electronic band structure proposed by Kuwamoto *et al.* (*18*). This model places the Fermi level in pure V_2O_3 near a local minimum in the density of states curve in the conduction band. This band is formed by the V^{3+} d orbitals, which lead to vanadium–vanadium bonding in the basal plane and possibly along the three-fold directions as well (in view of the close V–V approach along this axis). As Cr^{3+} is smaller, its substitution for V^{3+} produces ineffective orbital overlap and causes the removal of bonding states in the host lattice. Consequently, bonding electrons are effectively removed and the metal–metal distances increase. Additionally the removal of these states narrows the bands, resulting in a rapid deepening of the minimum. Macroscopically, the loss of states at the minimum is manifested by a pronounced increase in the resistance of the material at room temperature. With sufficient Cr^{3+} doping, the minimum is transformed into a gap, thereby creating an insulator. Addition of the larger Ti^{3+} need not result in deletion of states from the conduction band. However, Ti^{3+} is a d^1 ion while V^{3+} is a d^2 ion, thus substitution with Ti^{3+} also results in a decrease in the number of valence electrons in the band and an increase in the metal–metal distances. The Fermi level in these solid solutions is lowered from the minimum to give partially filled, normal bands for a metal.

Band crossing is not required by the Kuwamoto–Honig–Appel model, so the basic intermetallic bonding in doped V_2O_3 samples is not changed. Although bonding in the basal plane would be weakened somewhat, it would still be retained. The retention of an anisotropic metal–metal interaction in these materials is suggested by the behavior of the c/a ratio upon doping.

A plot of c/a versus average cation radius ($r_{M^{3+}}$) is linear (*19*) for those corundum structures which do not exhibit anomalous electric behavior (points 1–10 in Fig. 3). Those sesquioxides with anisotropic metal–metal interactions exhibit anomalously high or low c/a values. The metal–metal interaction along the c axis in Ti_2O_3 at room temperature results in a low c/a value for this compound. Upon heating from 100 to 300°C, Ti_2O_3 undergoes a gradual semiconductor-to-metal transition (*20*). In the band-crossing model of this transition (*21*), the metal–metal interactions become more isotropic. This is reflected in the structural changes accompanying the transition [the M(1)–M(2) distance increases while the longer M(1)–M(3) distance remains approximately constant, Ref. (22)] and in the more normal values of the c/a ratio for Ti_2O_3 above the transition temperature (open squares labeled 348 and 440° in Fig. 3). A gradual semiconductor-to-metal transition also accompanies doping Ti_2O_3 with increasing amounts of V_2O_3 (*23*). $(Ti_{0.9}V_{0.1})_2O_3$ exhibits metallic behavior and has a structure (*8*) which is similar in its dimensions to that of Ti_2O_3 above 300°C. The c/a value of this doped Ti_2O_3 system is also consistent with a more normal corundum structure.

The high c/a ratio of V_2O_3 has been attributed (*17*) to metal–metal interactions in the basal plane. Addition of Ti_2O_3 or Cr_2O_3 [Fig. 2, Tables II and III, Refs. (5, 8, and 11)] or heating pure V_2O_3 (*5*) appears to weaken these interactions; however, even at 50% Ti_2O_3, 5% Cr_2O_3, or 600°C the c/a ratio is still anomalously large compared to the behavior of other systems. Apparently some component of the anisotropic metal–metal interactions in the basal plane is retained under these conditions.

Acknowledgments

We wish to thank Professors J. M. Honig and J. Appel for helpful discussions. This work was supported by the National Science Foundation MRL Program through Grants 77-23798 and 80-20249.

References

1. R. M. Moon, *J. Appl. Phys.* **41,** 883 (1970).
2. P. D. Dernier and M. Marezio, *Phys. Rev. B* **2,** 3771 (1970).
3. J. Feinlieb and W. Paul, *Phys. Rev.* **155,** 841 (1967).
4. D. B. McWhan and J. P. Remeika, *Phys. Rev. B* **2,** 3734 (1970).
5. W. R. Robinson, *Acta Crystallogr. Sect. B* **31,** 1153 (1975).
6. G. V. Chandraskekhar, S. H. Shin, A. Jayaraman, J. E. Keem, and J. M. Honig, *Phys. Status Solidi A* **29,** 323 (1975).
7. R. E. Loehman, C. N. R. Rao, and J. M. Honig, *J. Phys. Chem.* **73,** 1781 (1969).
8. C. E. Rice and W. R. Robinson, *J. Solid State Chem.* **21,** 145 (1977).
9. D. B. McWhan, A. Menth, J. P. Remeika, W. F. Brinkman, and T. M. Rice, *Phys. Rev. B* **7,** 1920 (1973).
10. G. M. Joshi, H. V. Keer, H. Kuwamoto, and J. M. Honig, *Indian J. Pure Appl. Phys.* **15,** 471 (1977).
11. P. D. Dernier, *J. Phys. Chem. Solids* **31,** 2569 (1970).
12. J. C. C. Fan and T. B. Reed, *Mater. Res. Bull.* **17,** 1403 (1972).
13. H. V. Keer, D. L. Dickerson, H. Kuwamoto, H. L. C. Barros, and J. M. Honig, *J. Solid State Chem.* **19,** 95 (1976).
14. D. E. Williams, "LCR-2, A Fortran IV Lattice Constant Refinement Program," IS-1052, Iowa State University, Ames (1964).
15. L. W. Finger, "RFINE-2, A Fortran IV Program for Structure Factor Calculation and Least Squares Refinement of Crystal Structures," Geophysical Laboratory, Washington, D.C. (1972).
16. D. T. Cromer and J. T. Weber, *Acta Crystallogr.* **18,** 104 (1965).
17. J. B. Goodenough, *Prog. Solid State Chem.* **5,** 284 (1971).
18. H. Kuwamoto, J. M. Honig, and J. Appel, *Phys. Rev. B* **22,** 2626 (1980).
19. C. T. Prewitt, R. D. Shannon, D. B. Rogers, and A. W. Sleight, *Inorg. Chem.* **8,** 1985 (1969).
20. F. J. Morin, *Phys. Rev. Lett.* **3,** 34 (1959).
21. J. B. Goodenough, *Phys. Rev.* **117,** 1442 (1960).
22. C. E. Rice and W. R. Robinson, *Acta Crystallogr. Sect. B* **33,** 1342 (1977).
23. G. V. Chandrashekhar, Q. Won Choi, J. Moyo, and J. M. Honig, *Mater. Res. Bull.* **5,** 999 (1970).